Projecting End-of-Century Human Exposure from Tornadoes and Severe Hailstorms in Eastern Colorado: Meteorological and Population Perspectives

SAMUEL J. CHILDS AND RUSS S. SCHUMACHER

Department of Atmospheric Science, Colorado State University, Fort Collins, Colorado

STEPHEN M. STRADER

Department of Geography and Environment, Villanova University, Villanova, Pennsylvania

(Manuscript received 9 December 2019, in final form 19 May 2020)

ABSTRACT

Severe convective storms along the Front Range and eastern plains of Colorado frequently produce tornadoes and hail, leading to substantial damage and crop losses annually. Determination of future human exposure from these events must consider both changes in meteorological conditions and population dynamics. Projections of EF0 + tornadoes (on the enhanced Fujita scale) and severe [1.0+ in. (25.4+ mm)] hail reports out to the year 2100 are computed using convective parameter proxies generated from dynamically downscaled GFDL Climate Model, version 3 (GFDL CM3), output by the WRF Model for control and future climate scenarios. The proxies suggest that tornado and hail days in the region may increase by up to one tornado day and three hail days per year by 2100, with the greatest increases across northeastern Colorado. Using a spatially explicit Monte Carlo model, projected future frequency and spatial changes in tornadoes and hail are superimposed with population projections from the shared socioeconomic pathways (SSPs) to provide a range of possible scenarios for end-of-century human exposure to tornadoes and hailstorms. Changes in hazard frequency and spatial distribution may amplify human exposure up to 117% for tornadoes and 178% for hail in the region by 2100, although specific results are sensitive to uncertain combinations of future overlaps between hazard spatial distribution and population. Findings presented herein not only will provide the public, insurers, policy makers, land-use planners, and researchers with estimates of potential future tornado and hail impacts in the Front Range region, they also will allow the weather enterprise to better understand, prepare for, and communicate tornado and hail risk to eastern Colorado communities.

1. Introduction

Tornadoes and severe hailstorms are two of nature's most destructive and costly phenomena. In 2018 alone, 50% (7 of 14) billion-dollar disasters in the United States were attributed to tornado and severe hail events, two of which were hailstorms in eastern Colorado (Smith 2019). Even with laudable advancements in forecasting skill and warning messaging for tornadoes and severe hailstorms, significant damage and, in some cases, injuries and fatalities, still occur (Ashley 2007; Ashley and Strader 2016; Martius et al. 2018; Prein and Holland 2018; Sobel and Tippett 2018). The extent to which severe weather hazards will change in frequency and location in the future owing to climate change is an ongoing research question (Trapp et al. 2007; Brooks 2013; Diffenbaugh et al. 2013; Gensini and Mote 2015; Tippett et al. 2015; Hoogewind et al. 2017). Assessment of future human risk from these hazards must consider not only meteorological variables that prime the atmosphere for severe weather but also the numerous socioeconomic factors that affect the public's ability to receive and respond to warning messages, as well as cope with the impacts (Changnon et al. 2000; Pielke and Mills 2005; Bouwer 2011; Ashley et al. 2014; Visser et al. 2014; Strader et al. 2017). These societal factors also influence the evolution of population and development patterns and thus the number of people exposed to tornadoes and severe hailstorms.

This research aims to quantify the contributions of both meteorology and population dynamics to human exposure to tornadoes and hailstorms out to the end of the twenty-first century using Monte Carlo methods for the localized domain of eastern Colorado. Specifically, we ask, ''How many people in eastern Colorado will be

Corresponding author: Samuel J. Childs, sjchilds@rams.colostate.edu

DOI: 10.1175/WCAS-D-19-0153.1

in harm's way of tornadoes and hailstorms in the future compared to the present day?'' and ''How do the respective projected changes in meteorology and population contribute to the changing exposure?''

Within natural hazards literature, there are multiple definitions and meanings for many of the terms used herein (Paul 2011). We elect to follow the framework of the Intergovernmental Panel on Climate Change (IPCC) Special Report on Managing the Risks of Extreme Events and Disasters to Advance Climate Change Adaptation (SREX), which defines overall hazard *risk* as the interaction between hazardous weather and *impacts* as the potential negative effects consequent from the hazard (National Research Council 2009; IPCC 2012). Three elements contribute to risk, including *exposure*, which, as the main focus of this study, we define as the number of persons potentially affected by tornadoes or severe hailstorms (Strader et al. 2017). *Vulnerability* is defined as the susceptibility of a person or system to experience harm from a hazard and often includes the constructs of *sensitivity* and *adaptive capacity* (Cutter et al. 2000; Morss et al. 2011). The third element is simply the *hazard* itself, which we contextualize as the climatological probability of a tornado or hailstorm occurring in space and time (Morss et al. 2011; IPCC 2012).

Many prior studies have examined human exposure to severe weather hazards. For example, Bouwer (2013) found that flash flood and hurricane losses due to human exposure outweigh losses due to anthropogenic climate change out to the year 2040. Losses due to hailstorms are increasing globally in large part due to the expansion of the built environment (Changnon 2009; Prein and Holland 2018; Bouwer 2019). Similarly, Ashley et al. (2014) coined the ''expanding bull's-eye effect,'' which describes how population growth and the expansion of the built environment or urban sprawl has led to increased hazard impact frequency and magnitude on society. This effect has been linked to an increased tornado disaster potential in the Chicago, Illinois, metropolitan area (Ashley et al. 2014) and five other U.S. cities (Rosencrants and Ashley 2015). In addition, Strader et al. (2017) projected a threefold increase in tornado disaster potential by 2100 from a combined increase in tornado occurrence and the built environment (i.e., housing units) footprint. This research builds upon previous work in several ways. For one, severe hail is considered in addition to tornadoes, which represents a hazard that has shown increasing potential for loss, and, in some regions such as eastern Colorado, an increase in number of reports, days, and hailstone diameter, in recent decades (Allen et al. 2015a; Childs and Schumacher 2019; Trapp et al. 2019). A more realistic spatial representation of human exposure is considered through high-resolution shared socioeconomic pathway (SSP) population scenarios as well as projected frequency and spatial distributions of tornadoes and severe hail using high-resolution dynamically downscaled climate model output for control and future climate scenarios. Moreover, the small domain of eastern Colorado (37°–41°N, 102°–105.3°W; Fig. 1) offers an excellent example of the cumulative effects that meteorology and population can have on a local population that may not be gleaned from studying a broader area.

FIG. 1. Location of the eastern Colorado domain that is considered in this study (37°–41°N, 102°–105.3°W).

Eastern Colorado has an intriguing severe weather climatology unique from other well-known severe weather regions of the United States. Here, a moist boundary layer, directional wind shear, and local topographical complexities contribute more to severe weather as opposed to very large convective available potential energy (CAPE) and vertical wind speed shear typically associated with severe weather environments farther east (Doswell 1980; Maddox et al. 1981; Szoke et al. 1984). Nonmesocyclonic tornadoes and landspouts are common in this area due to features such as the Denver convergence vorticity zone (DCVZ) and associated Denver Cyclone that were discovered as a result of several field projects in the 1980s (Szoke et al. 1984; Wilson et al. 1988; Brady and Szoke 1989). This region of enhanced vorticity forms on many spring and summer days when low-level southeasterly winds ascend the Palmer Divide south of Denver and collide with northwesterly winds traversing downslope off the foothills, setting up a convergence zone in which tornadoes can spin up in the absence of strong midlevel rotation.

Multiple studies have identified eastern Colorado as a local maximum in both tornado (Brooks et al. 2003a;

Ashley 2007; Allen et al. 2015b; Farney and Dixon 2015; Childs and Schumacher 2019) and severe hail events (Changnon 1999; Cintineo et al. 2012; Allen and Tippett 2015; Childs and Schumacher 2019). Multiple destructive hail events have occurred across eastern Colorado in recent years, including the 9 May 2017 Denver hailstorm that became the costliest in state history at $2.3 billion (Rocky Mountain Insurance Information Association 2019), the 6 August 2018 Cheyenne Mountain Zoo hailstorm that injured 12 people (Childs and Schumacher 2018b), and the 13 August 2019 hailstorm in rural eastern Colorado that produced a new state record 4.83 in. (122.7 mm) hailstone (Schumacher 2019). Although tornadoes in eastern Colorado are often weak (e.g., enhanced Fujita scale EF0 or EF1) and nonmesocyclonic, two fatality-producing tornadoes have impacted the state in the twenty-first century.

The population dichotomy across eastern Colorado also affirms the region as one of particular interest in assessing exposure to tornadoes and severe hail. The Front Range urban corridor, from Pueblo north to Fort Collins, continues to experience rapid population growth; however, many counties on the eastern plains have seen very little population growth over time and are projected to have either neutral or slightly decreasing population by 2040 (Colorado State Demography Office 2012). Nevertheless, tornado and hail impacts in the region are felt area-wide, with physical damage and human injuries of main concern across urban areas and significant crop losses in the more agrarian communities.

While this study is focused on eastern Colorado, the methods presented herein may be applied to other localized regions of the country, if desired. Assessing natural hazard risk and societal vulnerability across a larger spatial domain is certainly helpful in providing large-scale patterns and allowing for influences such as climate change to be considered more appropriately, but localized analyses such as those conducted in this study appeal to the ''me factor'' that points to the desire for an individual to know exactly what is going to happen to him or her in a hazard event (Nagele and Trainor 2012; Morss et al. 2016; Childs and Schumacher 2018a). This is especially true in a region such as eastern Colorado, where vibrant crop and ranching communities adjacent to a rapidly developing metropolitan area both experience damaging severe weather events.

The remaining portions of this manuscript are outlined as follows: section 2 introduces the structure of the Monte Carlo models that are used to simulate human exposure to tornadoes and severe hailstorms. The methods and creation of the two main components that are ingested into the models are then motivated and described, including the spatial population projections in section 3 and the tornado and severe hail weighting surfaces from dynamically downscaled climate model output in section 4. Results from the Monte Carlo simulations are presented in section 5 and give a range of possible changes in human exposure based on climatological and population scenarios. Section 6 offers some application and implications of the projected human exposure, and section 7 concludes with a summary of key findings and motivation for future work.

2. Tornado and hail Monte Carlo models

Monte Carlo (MC) statistical approaches draw upon random numbers and probability to repeatedly sample and run statistics on a population to give estimated solutions (Mooney 1997). MC methods have been applied to a variety of problems in the atmospheric sciences from reflectivity of clouds (Barker et al. 2003) to precipitation impacts on aerosols (Zhao and Zheng 2006) and uncertainty estimates of disaster costs (Smith and Matthews 2015). To explore the impacts of population and tornado statistics on the human and the built environment, the Tornado Monte Carlo (TorMC) model was developed by and described at length in Strader et al. (2016). TorMC has proven utility in projecting future changes in tornado exposure over large areas the country. For example, both Strader et al. (2016) and Strader et al. (2017) illustrate that physical exposure, as measured by housing units, outweighs frequency of tornado events in its contribution to disaster severity. This study applies TorMC to the localized eastern Colorado domain to assess the contributions of population dynamics and climatological changes to human exposure by the year 2100. In addition, a Hail Monte Carlo (HailMC) model is developed using the framework of TorMC to investigate human exposure from severe hailstorms (Fig. 2).

TorMC and HailMC are composed of multiple user inputs followed by a simulation. The user must designate the desired magnitude range of the hazard to be simulated, in this case the EF-scale rating for tornadoes and hailstone diameter. For the eastern Colorado domain considered, all EF-scale ratings are considered for tornadoes, as 96% of all tornado reports since 1997 have been of the (E)F0 or (E)F1 variety (Childs and Schumacher 2019). Although the U.S. (E)F0 tornado record shows a nonmeteorological jump in the 1990s due to the implementation of Doppler radar (Verbout et al. 2006; Agee and Childs 2014), for the temporal and spatial domain considered here, this artifact is largely absent, as TorMC samples only those tornadoes within the eastern Colorado domain. For HailMC, the severe threshold of 1.0 in. (25.4 mm) used by the

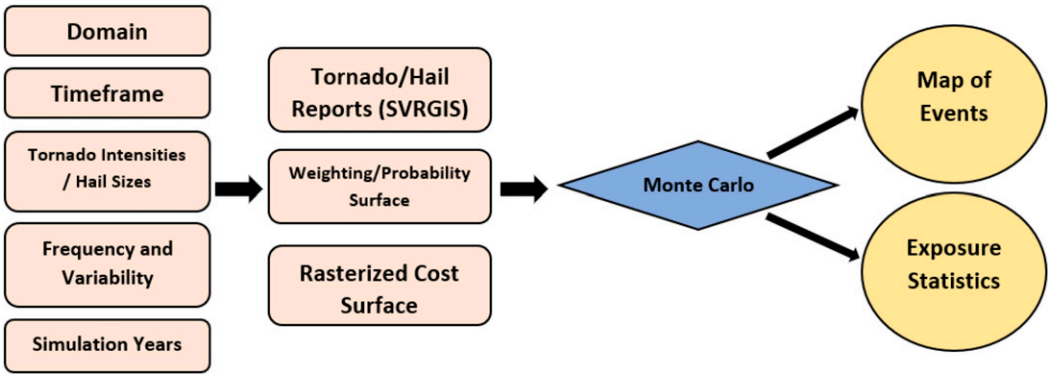

FIG. 2. The basic structure of the TorMC and HailMC models. The far-left rectangles represent basic user inputs, and the next column of rectangles shows the shapefiles and raster files that are created and input to the model (diamond). The ovals represent the output from the Monte Carlo simulations, namely, a plot of tornado paths or hail swaths, as well as human exposure statistics.

National Weather Service (NWS) is employed. While the number of significant [2.0+ in. (50.8+ mm)] hail reports in eastern Colorado is increasing over time (Childs and Schumacher 2019), they account for only 6.5% of all severe hail reports, and the relative change in human exposure from HailMC was found not to be sensitive to the selection of minimum hailstone size. The range of years over which to select tornado and/or severe hail historical reports is also entered. This study uses the period 1997–2017, which represents the Doppler radar era characterized by much higher tornado and hail data reliability compared to previous years (Verbout et al. 2006; Agee and Childs 2014; Allen and Tippett 2015).

TorMC and HailMC also ingest two shapefiles: 1) the domain of interest, in this case eastern Colorado (37°–41°N, 102°–105.3°W), and 2) GIS files of the initial points of tornado and severe hail reports, accessed from the Storm Prediction Center's (SPC) Severe Weather GIS (SVRGIS). Raster surfaces must be created and input into the MC models. A control weighting surface for each hazard represents a spatial probability of tornado and severe hail occurrence based on the historical distribution of reports over the 1997–2017 control period. A future weighting surface is also created, as described in section 4, to represent the projected future spatial distribution of these hazards across eastern Colorado. Rasterized cost surfaces of human statistics—in this case, a control population surface for the year 2000 from the 1-km Gridded Population of the World (GPW), version 3, dataset and five 1-km SSP, version 1.1, population projections for 2100—are also input into the models (available online at http://www.cgd.ucar.edu/iam/modeling/spatial-population-scenarios.html).

For each year in the 1000-yr MC simulations for both control and future statistics, tornado paths and hail swaths are created by first "grabbing" a tornado or severe hail report according to the probabilistic weighting surface. In TorMC, each selected tornado is assigned a magnitude and length (km) from the database and a width (km) that fits a Weibull distribution according to its magnitude (Brooks 2004). A tornado azimuth, that is, its direction of travel, is selected randomly from a wider sample of all tornadoes in the CONUS for the 1997–2017 period to avoid a bias toward erroneous northerly azimuths in eastern Colorado. With these attributes, a tornado polygon geometry is created and placed onto an output data frame. HailMC proceeds similarly, with each simulated hail event assigned a diameter from eastern Colorado SPC reports. Severe hail reports are documented as occurring at a single point in space, but in reality, hail of the reported magnitude occurs in a swath surrounding the point. As such, HailMC assigns each simulated hail report a length and width of 0.1 km and an azimuth of zero, creating a square of hail. While hail often falls in longer and more irregular swaths or contains multiple sizes within the same swath, this study is concerned with *relative* changes in human exposure as opposed to absolute changes. In other words, hail swaths of equal sizes in the control and future simulations allow for a homogeneous comparison of potential impacts. Experiments were run using larger hail swaths, but the relative change in human impacts did not vary significantly.

Once all tornado or severe hail polygons are created, a 1-km cost surface of GPW or SSP population density is overlaid using the same coordinate reference system. The number of people underneath a polygon can then be computed for each scenario of interest. Numerous options exist for how to calculate human statistics within a gridded domain, but this study elects to define an entire grid cell as being affected if a tornado path or hail swath intersects any part of it (e.g., Fig. 4 from Strader et al.

TABLE 1. Summary of assumptions about population growth and urbanization level, and the resulting spatial pattern, for each of the five SSP scenarios, for given country statistics. Population growth levels are given according to fertility categories, where "high" indicates countries with birth rates in excess of 2.9, "other low" indicates countries with birth rates less than 2.9, and "rich low" indicates countries designated as a high income country by the World Bank with birth rates less than 2.9, for the period 2005–10 (Samir and Lutz 2017). Urbanization level is connected to current income levels for each county or region. This table is reproduced from Jones and O'Neill (2016).

	SSP1: sustainability	SSP2: middle-of-the-road	SSP3: regional rivalry	SSP4: inequality	SSP5: fossil-fueled development
Fertility			Population growth		
High	Low	Medium	High	High	Low
Other low	Low	Medium	High	Medium–low	Low
Rich low	Medium	Medium	Low	Medium–low	High
Income			Urbanization level		
High	Fast	Central	Slow	Central	Fast
Medium	Fast	Central	Slow	Fast	Fast
Low	Fast	Central	Slow	Fast	Fast
			Spatial pattern		
	Concentrated	Historical patterns	Mixed	Mixed	Sprawl

2016). In total, three simulations are run for each hazard: a control run, one with a uniform amplification of tornado and severe hail reports across the domain and the control weighting surface, and one with uniform amplification of tornado and severe hail reports and the future weighting surface. The control cost surface and each of the five SSP projections are then overlaid on each simulated tornado and hail landscape to give a range of potential impacts.

3. Population dynamics

a. Background and approaches

The extent to which local, regional, and national population landscapes change is governed by a variety of factors. The U.S. Census Bureau conducts a national census on a decadal basis, amassing a wide variety of population statistics. These reports are useful for extracting broad trends of population at relatively coarse resolution (e.g., state level, regional, national). For finer-scale population statistics, many state demography offices can provide county-level, block-level, or neighborhood-level data. For long-range population projections under different scenarios, a number of datasets have been developed. These include the IPCC's Special Report on Emissions Scenarios (SRES; Nakićenović and Swart 2000), Integrated Climate and Land Use Scenarios (ICLUS; U.S. EPA 2016), and SSPs (O'Neill et al. 2013). The five SSPs are based on national-level projections of various sectors such as economics, education, technology, and immigration, and are meant to provide a measure of how a society will be able to adapt to and mitigate the influences of a changing climate (Jones and O'Neill 2013, 2016). Thus, the SSPs have gained a particular following in natural hazards research (Ebi et al. 2014). Specifically, the five SSPs are labeled as sustainability (SSP1), middle-of-the-road (SSP2), regional rivalry (SSP3), inequality (SSP4), and fossil-fueled development (SSP5). Table 1 depicts a slightly modified table from Jones and O'Neill (2016) showing the broad demarcations of population growth and urbanization levels of the five SSP projections. The reader is directed to Jones and O'Neill (2016) for additional background on the SSPs and other population scenarios.

Jones and O'Neill (2016) created a set of global spatial population projections in decadal increments out to 2100 that are both qualitatively and quantitatively consistent with the SSPs. Gao (2017) describes a gravity model-based downscaling approach to map spatial patterns and their changes over the United States. In short, the 1/8° SSP projections are downscaled to a 1-km grid using a 1-km population count from the Global Urban-Rural Mapping Project (GRUMP), version 1 (Center for International Earth Science Information Network 2011), which incorporates the finest level census data available. An aggregation procedure then maps the 1-km GRUMP data onto 1/8° grid to match the SSP narratives. Finally, a 1-km weighting map is created to show how the coarser population is spread among the 1-km grid cells, which is then multiplied to the 1/8° projections. This method is followed by Jones and O'Neill (2016) to aggregate the GPW base case population surface to match the resolution of the SSPs. Gao (2017) cautions that "subtle spatial artifacts" exist in the 1-km population projection maps, but these are generally found outside of North America, where population statistics are less reliable. Nevertheless, the 1-km results were cross validated with 1/8° resolution for the domain of interest, and only minute changes were found in relative

population changes across eastern Colorado that do not affect the overall conclusions.

b. *Eastern Colorado projections*

The base case population used in the SSP framework is taken from the GPW 1-km dataset for 2000 (Fig. 3). The end-of-century, downscaled 1-km SSP projections are clipped to the Colorado state boundary using GIS. Each SSP scenario evolves differently over time according to its underlying socioeconomic assumptions (Fig. 4). None of the SSP scenarios predict much population change over the eastern plains, but distinct features are noted along the Front Range urban corridor. For example, SSP5 produces enormous population growth in the Front Range cities (greater than 50 000 persons in many adjacent grid boxes) and also expands suburbs in areas north of Colorado Springs, fills in gaps between Denver and Castle Rock to the south and Fort Collins to the north, and increases the population along and east of Interstate 25 in northern Colorado. In this scenario, the reliance on fossil fuels continues to spur development; income growth, innovation, and investments in education are high; and a large number of migrants come to the United States for work. As such, rapid urbanization occurs, with a spatial pattern of population extensions around metropolitan areas (Jones and O'Neill 2016).

SSP1 (sustainability) and SSP2 (middle-of-the-road) scenarios are the most consistent with recent demographic trends, with modest income growth and migration, as well as investments in education and the environment. This results in a moderate increase in population along the Front Range urban centers with some east–west population extension in both SSP1 and SSP2. SSP4 shows a more muted response along the urban corridor as well as areas of decreasing population on the edges of cities. This scenario, coined ''inequality,'' is characterized by slow economic growth and a lack of opportunities in rural communities, favoring a more concentrated population in cities and industrial areas. Finally, SSP3 evolves in such a way as to project much less population along the urban corridor by 2100. The SSP3 scenario of ''regional rivalry'' represents economic uncertainty, security concerns, and low technological growth, leading to lower fertility in high-income countries. This results in a dying population, but also pockets of wealth beside slums in big cities as economic growth is stunted. It is also interesting to note how other smaller communities such as Fort Morgan and Sterling on the eastern plains are projected to grow in all scenarios except SSP3 (Fig. 4), whereas the town of Limon is not expected to experience much growth under any scenario, perhaps due to its currently small industrial sector.

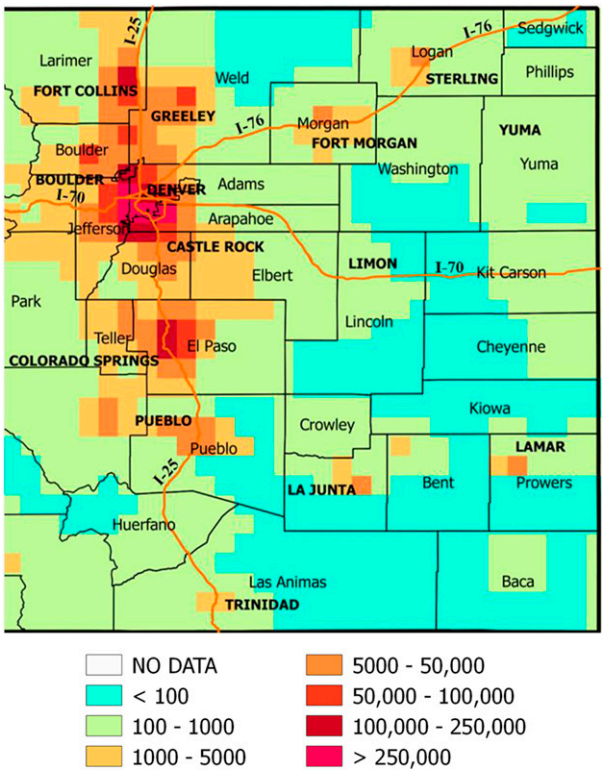

FIG. 3. Base case population density for 2000, taken from the GPW dataset at $^1/_8°$ gridded resolution. The units shown are number of persons per $^1/_8° \times {}^1/_8°$ grid box. County names are in regular font type, select cities are uppercase boldface, and interstate highways are marked by orange lines.

To summarize, numerous factors must be considered in projecting end-of-century population density, including immigration, education, foreign relations, technological growth, and local factors specific to Colorado that are not explicitly accounted for in dataset used here (Jones and O'Neill 2016). Each of the five SSPs predict population growth over most areas relative to the GPW base case scenario, especially along the Front Range urban corridor. However, there are subtle differences in how cities are projected to expand and also in the relative growth of smaller towns on the eastern plains. While the likelihood of a single SSP projection materializing is slim, the takeaway message is that a wide range of population scenarios for eastern Colorado exists, which consequently impacts the number people who may be exposed to tornadoes and severe hail in the future.

4. Projection of tornado and hail probabilities

a. *Background and approaches*

A combination of favorable environmental ingredients must exist in sufficient quantities for the formation

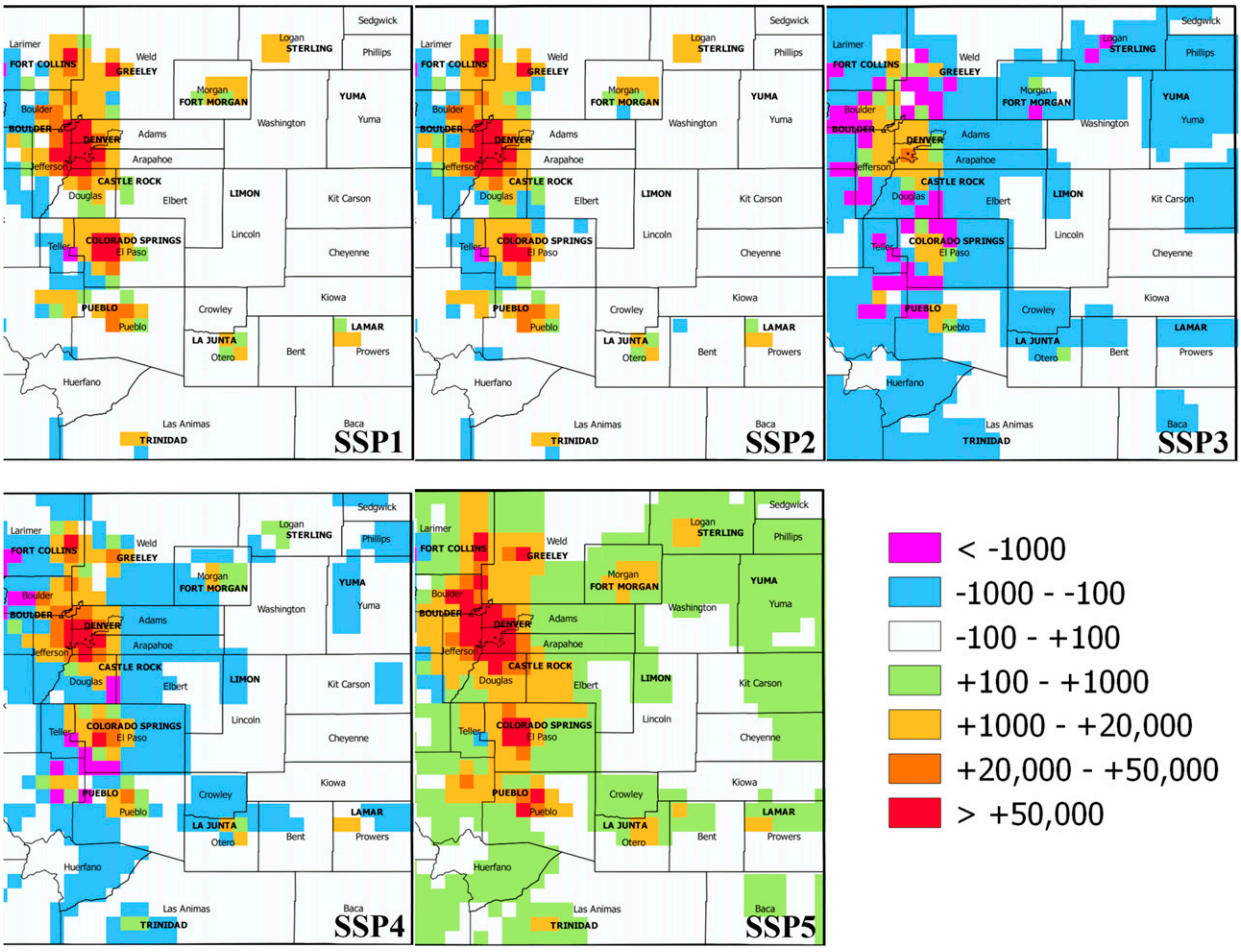

FIG. 4. Change in population between end-of-century SSP projections and the GPW year-2000 base case population at 1/8° resolution.

of a thunderstorm capable of producing large hail and tornadoes. These ingredients most foundationally include instability, vertical wind shear, moisture, and a lifting mechanism (Brooks et al. 2003b; Brooks 2009; Allen et al. 2015a; Tippett et al. 2015). An environment that is favorable for tornadoes is not necessarily favorable for large hail, due in part to the complex microphysical aspects of hail growth and its dependence on environmental temperature and moisture profiles (Rasmussen and Pruppacher 1982; Edwards and Thompson 1998; Allen et al. 2015a; Prein and Holland 2018; Trapp et al. 2019), so it is worthwhile to project probability of these two hazards separately.

Two main approaches have surfaced to assess long-term prediction of severe weather: 1) the "ingredients-based approach," which analyzes trends in well-known severe weather parameters; and 2) the "synthetic reports approach," which simulates severe weather events using proxy thresholds. The ingredients-based approach has yielded a general consensus that as the climate warms and moistens, CAPE will increase and vertical wind shear will decrease (e.g., Trapp et al. 2007; Brooks 2013; Diffenbaugh et al. 2013; Seeley and Romps 2015), but the decrease in shear occurs on days in which CAPE is negligible (Diffenbaugh et al. 2013), yielding an overall more favorable future severe weather environment. This conclusion, however, may not apply to all regions, and does not partition according to particular severe weather hazards. Recent work has applied the ingredients-based approach using a pseudoglobal warming framework, in which a high-emissions (RCP8.5) climate perturbation is applied to high-resolution dynamical downscaling of climate models to compare with control scenarios. These studies have generally affirmed a greater potential for hazardous convective weather across the eastern two-thirds of the country in the future owing to concurrent increases in CAPE and convective inhibition (CIN) as well as enhanced moisture transport (Rasmussen et al. 2020; Chen et al. 2020), although simulations by Trapp and Hoogewind (2016) that aimed to isolate tornadoes

failed to produce any convection due to high CIN. A warmer atmosphere also means higher melting levels, which would favor melting of the smallest hailstones on their descent to the surface (Xie et al. 2010); however, the largest hailstones with relatively fast terminal velocities are not affected as much by melting and thus may become preferential to smaller hail in reaching the surface (Mahoney et al. 2012; Dessens et al. 2015; Brimelow et al. 2017).

The synthetic reports approach to severe storm analysis and forecasting, also called "surrogate severe" (Sobash et al. 2008), is grounded by the argument that any trend in favorable severe weather environments is dependent upon those environments being realized in a future climate. In this framework, dynamical downscaling of climate model output onto a fine grid using weather models such as WRF is performed to create synthetic severe reports from proxy parameters. Common parameters for general severe weather include a combination of updraft helicity and reflectivity (UH–*Z*; Trapp et al. 2011; Gensini and Mote 2014, 2015), UH and CAPE (Robinson et al. 2013), UH (Sobash et al. 2016; Sobash and Kain 2017), and upward vertical velocity (UVV; Hoogewind et al. 2017). In addition, UH has proven useful for tornadoes (Clark et al. 2013; Gallo et al. 2016), and column-integrated graupel (GRPL) for severe hail (Sobash et al. 2011; Trapp et al. 2019).

This study employs the synthetic reports approach using model output from Hoogewind et al. (2017). The global climate model employed is the Geophysical Fluid Dynamics Laboratory Climate Model, version 3 (GFDL CM3; Donner et al. 2011), with the RCP8.5 scenario applied to phase 5 of the Coupled Model Intercomparison Project (CMIP5; Taylor et al. 2012) used for historical and future simulations. Two 30-yr periods are compared representing historical (1971–2000) and future (2071–2100) climates. The GFDL CM3 model is downscaled using WRF-ARW, version 3.6, which is reinitialized each day and gives output every hour over the entire CONUS at 4-km horizontal grid spacing. For a thorough description of the model setup, see Hoogewind et al. (2017). The convective proxies include hourly maxima of 2–5-km UH, UVV (in the lowest 400 hPa), GRPL, and the Air Force Weather Agency Tornado (AFWATor) and Hail (AFWAHail) parameters. The AFWA parameters are part of a larger group of diagnostics used in the AFWA Mesoscale Ensemble Prediction Suite, which were incorporated into WRF starting with version 3.6 (Creighton et al. 2014) and have been used in various simulations of severe weather events (Martynov et al. 2017; Yavuz et al. 2017) and the 2017 NOAA Hazardous Weather Testbed (Gallo et al. 2017). The AFWATor parameter is a measure of the maximum tornado wind speed ($m\,s^{-1}$), and the AFWAHail parameter approximates the maximum hailstone size (see Creighton et al. 2014 for formal definitions). Traditionally in synthetic report creation, some threshold is assigned to the parameter of interest, and a 24-h period in which that threshold is exceeded over some domain constitutes a day in which that particular severe weather hazard occurred. This allows a comparison to be made between severe weather days in historical and future climates.

b. Eastern Colorado projections

To create the control (CTRL) weighting surfaces for use in the MC models, the SPC tornado and severe hail reports for the period 1997–2017 are first upscaled to a 0.25° latitude by 0.275° longitude grid across the domain, a procedure that helps to offset the errors associated with the placement of local storm reports in the SPC database due to population bias (Hoogewind et al. 2017; Trapp et al. 2019). The annual average number of tornado and severe hail days within each box is then calculated, and the grids are converted to shapefiles and then rasterized (Fig. 5). Even in this period of relative data reliability, tornado and particularly severe hail days show a bias toward population centers along the Front Range, a phenomenon that has been affirmed in various studies (Allen and Tippett 2015; Potvin et al. 2019; Childs and Schumacher 2019).

Creation of future (FUT) weighting surfaces begins by finding the 99.99 percentile of each selected convective parameter in the WRF output across the domain for the CTRL period (1971–2000). The percentiles are then adjusted in one-unit increments until the number of days in which the threshold is exceeded at least somewhere in the domain most closely matches the 508 tornado and 955 hail days from the SPC data records in the 1971–2000 CTRL period. For example, the 99.99 percentile for UH across the domain is $123.875\,m^2\,s^{-2}$. This value is adjusted downward to $97.875\,m^2\,s^{-2}$, which is exceeded on 513 days in the CTRL period and thus most closely matches the 508 tornado days. Each threshold value computed for the eastern Colorado domain are justified according to the literature or definitions (Table 2). These thresholds can provide an estimate of tornado and severe hail days in the CTRL period (1971–2000) by computing the average number of days of threshold exceedances, using AFWATor, UH, and UVV as tornado proxies (Fig. 6a) and AFWAHail, UH, UVV, and GRPL as severe hail proxies (Fig. 6b). These spatial distributions largely miss the nonmeteorological concentration of SPC reports along the urban corridor (Figs. 5a,b) since synthetic hazard days do not contain population bias. A few examples of observational and synthetic report alignment is evident, however, such as a

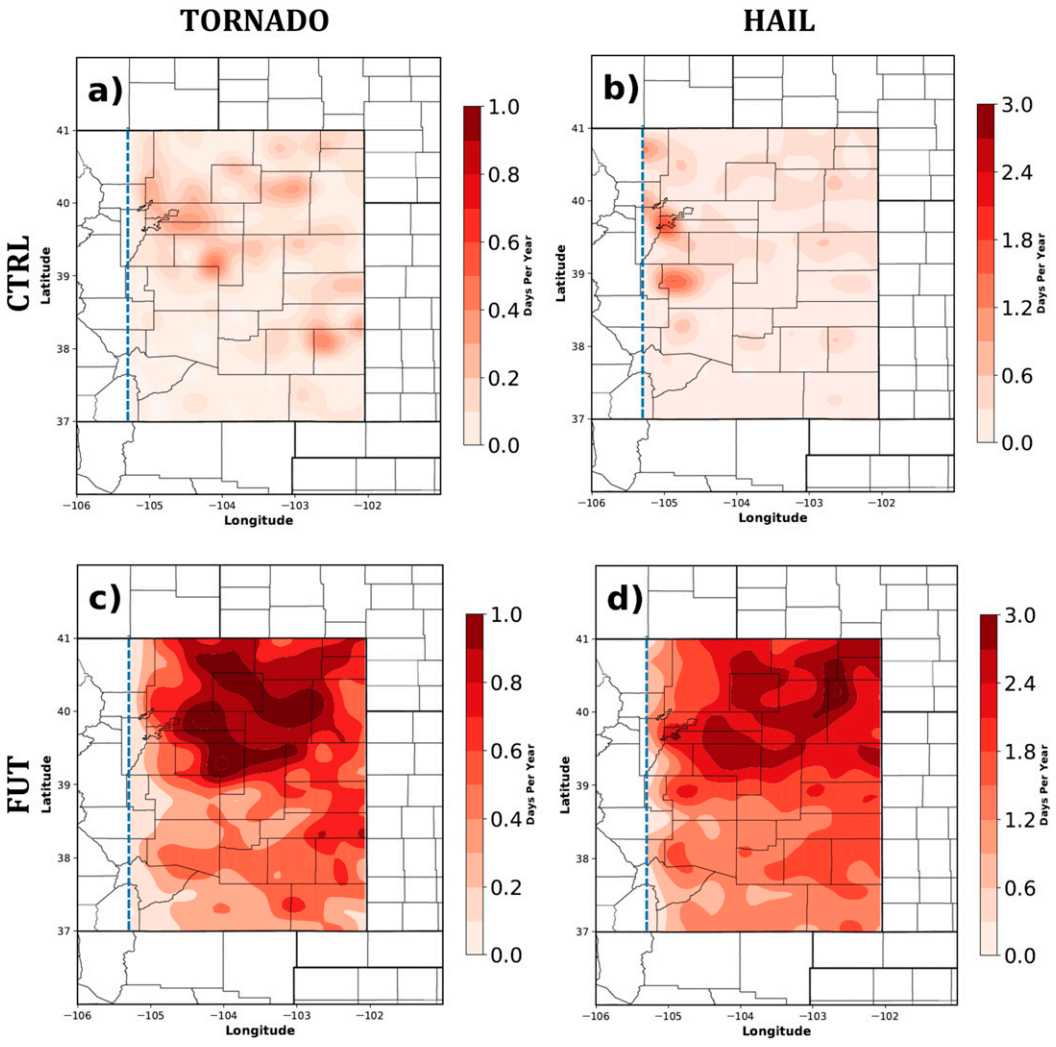

FIG. 5. Weighting raster surfaces for (left) tornado and (right) severe hail events across eastern Colorado. (a),(b) Control surfaces are based on 1997–2017 SPC local storm reports converted to tornado and severe hail days, and (c),(d) future surfaces are based on synthetic tornado and severe hail days projected for the period 2071–2100 from high-resolution WRF data output. Note that the contour intervals are not equivalent between the two hazards.

relative maximum in tornadoes near the town of Lamar in southeastern Colorado. Recent studies comparing observations of tornadoes (Gensini and Brooks 2018) and severe hail (Tang et al. 2019) also note a mismatch of favorable environments and SPC reports in the immediate lee of the Rocky Mountains, likely caused not only by population bias but also by the inability of models and reanalyses to correctly capture orographic effects. The approach taken here is to merge observations and synthetic days in creation of future hazard probabilities.

Following threshold computation, the 4-km WRF data output is upscaled to a 0.25° × 0.275° latitude–longitude grid over the eastern Colorado domain to match that of the tornado and severe hail days grids. The number of days that each parameter threshold is exceeded in each grid box over the CTRL (1971–2000) and FUT (2071–2100) periods is tabulated, with the restriction of only one exceedance per time step per grid box, even if multiple grid points within said box exceed the threshold. Each grid of threshold exceedance is divided by 30 to yield an annual average for both periods, after which the CTRL grid is subtracted from the FUT grid to give the difference in the annual number of threshold exceedances for each parameter. The resulting difference grids for AFWATor, UH, and UVV (Figs. 7a–c) are averaged for the tornado hazard (Fig. 7d), and the AFWAHail, UH, UVV, and GRPL difference grids (Figs. 8a–d) are averaged for severe hail (Fig. 8e) to give a measure of the projected spatial

TABLE 2. Thresholds of each severe weather parameter from WRF output used in the computation of eastern Colorado synthetic reports. Justification from other studies or definitions are given in the rightmost column.

Parameter	Computed threshold	Justification
UH ($m^2 s^2$)	97.875 (tornado); 69.875 (hail)	$100\,m^2\,s^{-2}$ used in predicting tornado pathlength (Clark et al. 2012); $\geq 60\,m^2\,s^{-2}$ found to be optimal for hazardous convective weather events (Gensini and Mote 2014); $\geq 40\,m^2\,s^{-2}$ used for severe weather occurrence (Trapp et al. 2007)
UVV ($m\,s^{-1}$)	26.0625 (tornado); 23.0625 (hail)	$22\,m\,s^{-1}$ found to be optimal for hazardous convective weather (Hoogewind et al. 2017)
AFWATor ($m\,s^{-1}$)	32.75	Near the middle of EF0 tornado wind speed range ($29–38\,m\,s^{-1}$)
AFWAHail (mm)	28.625	25.4 mm (1 in.) is SPC severe criterion
GRPL ($kg\,m^{-2}$)	26.4375	$25\,kg\,m^{-2}$ used as surrogate for 1-in. hail (Gagne et al. 2017; Sobash 2018); max values of $35–45\,kg\,m^{-2}$ found in case study of 23 Apr 2009 hail episode (Kain et al. 2008)

change in annual tornado and severe hail days for the 2071–2100 FUT period. Figures 7d and 8e reveal that occurrences of synthetic tornado and severe hail reports are projected to increase everywhere across the domain by 2100, with the northern half of eastern Colorado more active relative to the southern half. A similarly oriented arc of maximum annual increase in both hazards stretches across northeastern Colorado, from central Weld County, south to central Elbert County, east to Washington County, and northeast to Sedgwick County (Figs. 7d and 8e). South of Interstate Highway 70, the increase in annual synthetic report days is more muted, particularly for tornadoes, as almost all grid boxes in the southern half of the domain are projected to see an increase of less than one day per year. It is also apparent that annual severe hail days are projected to increase at least twice as much as tornadoes by the 2071–2100 period.

Individual convective parameters vary in their contribution to changing synthetic tornado and severe hail reports. In general, the UVV difference fields for tornadoes (Fig. 7c) and severe hail (Fig. 8c) show larger annual increases relative to the UH fields. The AFWATor (Fig. 7a) and AFWAHail (Fig. 8a) parameters share qualitative resemblance to the respective UH and UVV fields, as their formulas contain contributions from UH and UVV. The greatest magnitude of increasing threshold exceedance in the FUT period for either hazard is the GRPL parameter (Fig. 8d). Almost all grid boxes show at least one more day per year of GRPL threshold exceedance, with a bull's-eye of greater than 4 days per year just east of DIA. This result is

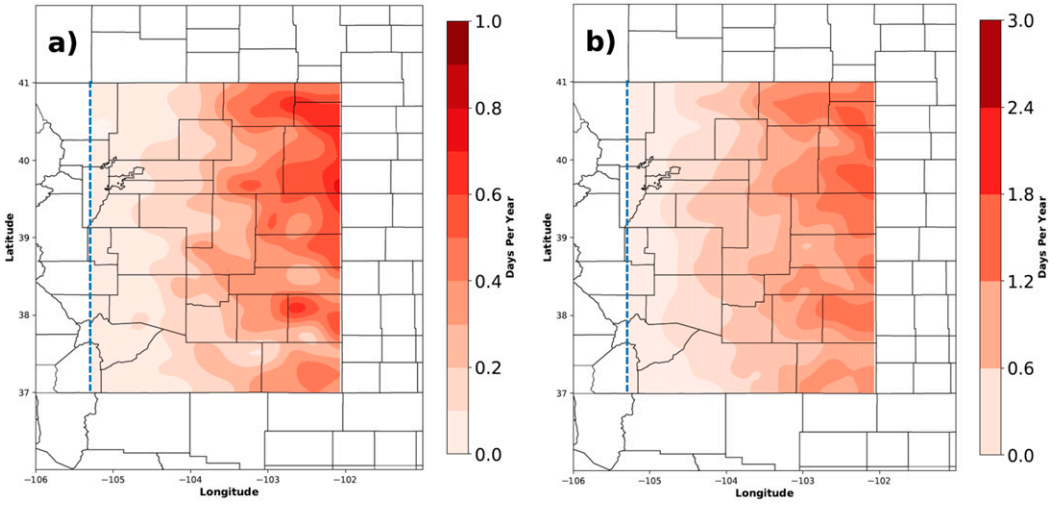

FIG. 6. Average number of annual synthetic (a) tornado and (b) severe hail days for the WRF Model CTRL period (1971–2000) over eastern Colorado. Tornado days are computed from an average of daily threshold exceedances of AFWATor, UH, and UVV; severe hail days are computed from an average of daily threshold exceedances of AFWAHail, UH, UVV, and GRPL. Note that the contour intervals are not equivalent between the two hazards.

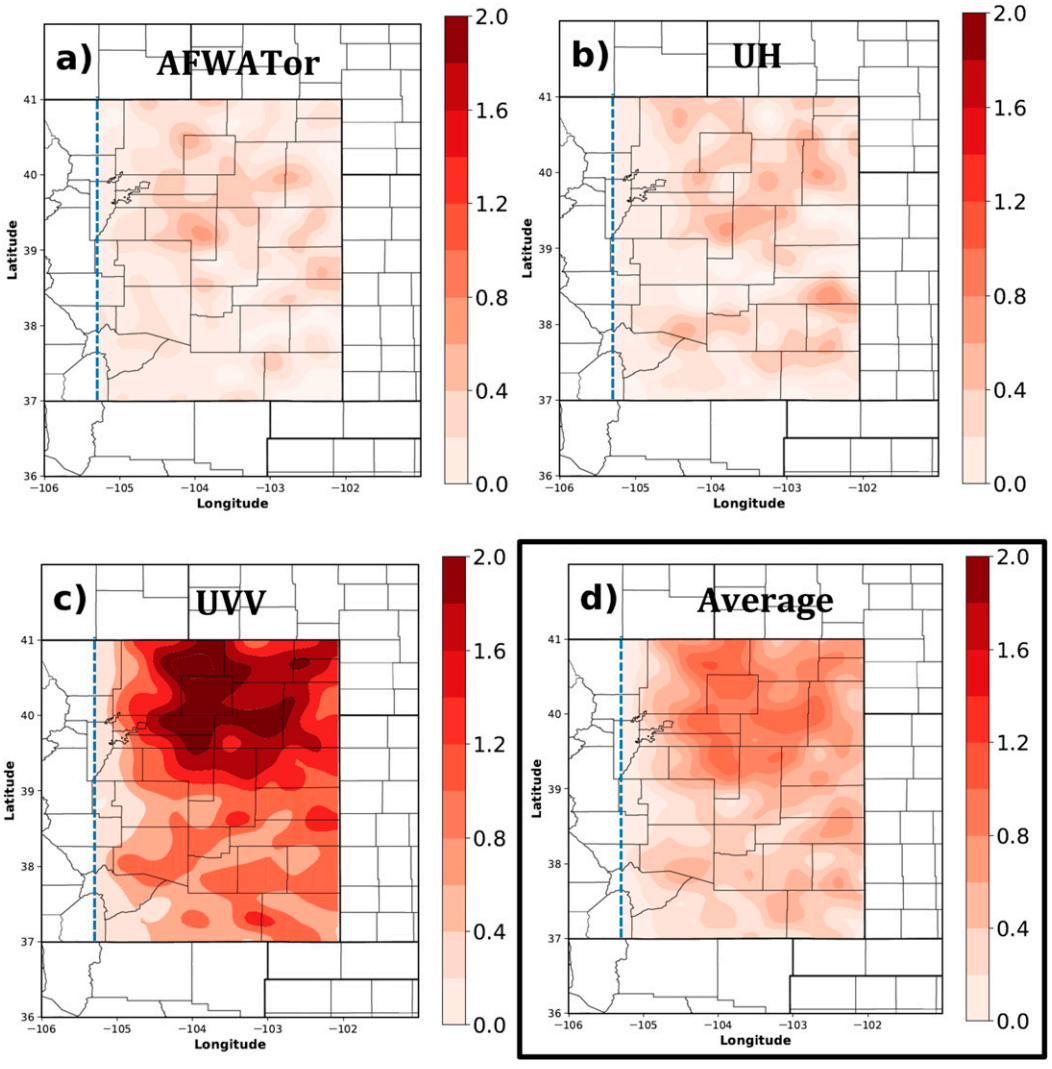

FIG. 7. Difference in the number of annual days in which (a) AFWAT or $> 32.75\,\mathrm{m\,s^{-1}}$, (b) UH $> 97.875\,\mathrm{m^2\,s^2}$, and (c) UVV $> 26.0625\,\mathrm{m\,s^{-1}}$ between the future (2071–2100) and control (1971–2000) periods. (d) The average of these three grids. Grid boxes are 0.25° latitude × 0.275° longitude.

consistent with Trapp et al. (2019) who showed projections of up to four days per each summer month of GRPL exceeding their large hail threshold of $25\,\mathrm{kg\,m^{-2}}$ across the western Great Plains on a coarser domain. It should be noted that since Figs. 7d and 8e represent averages of three and four proxies, the projected increase could be an underestimate. In addition, coarser resolution would yield a greater number of days per year of increase per grid box (Trapp et al. 2019).

Last, the synthetic tornado and hail grids are added to their respective CTRL weighting surface to form the FUT weighting surfaces used in the MC models (Figs. 5c,d). These weighting surfaces have a similar spatial distribution to Figs. 7d and 8e, and represent enhanced tornado and severe hail probabilities away from the urban corridor toward northeastern Colorado. Since the FUT weighting surface incorporates both synthetic reports, which is free from population bias, and the biased SPC storm reports used in forming the CTRL weighting surface, a more realistic picture of the future hazard landscape emerges. The percent change in the projected annual number of tornado and severe hail reports can also be calculated assuming a CTRL-period average of 2.45 and 5.88 tornadoes and severe hail reports per tornado and severe hail day, respectively. This yields increases of 2.9% more tornadoes and 3.5% more severe hail in the 2071–2100 FUT period, which are represented in the future MC experiments as an adjustment in tornado and severe hail annual counts. The small sample size of *significant* tornadoes and hail reports over this localized domain precludes analysis of changes

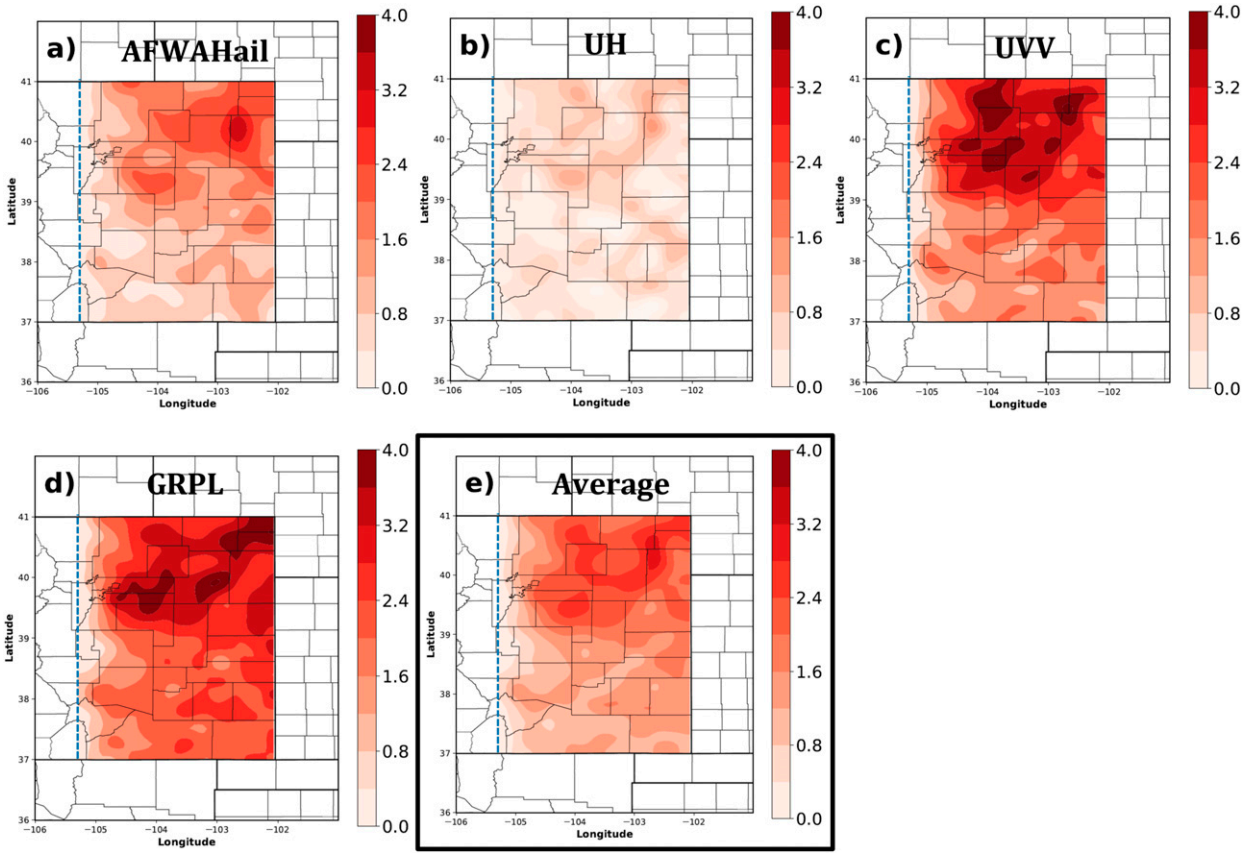

FIG. 8. Difference in the number of annual days in which (a) AFWAHail > 28.625 mm, (b) UH > 69.875 $m^2 s^2$, (c) UVV > 23.0625 m s^{-1}, and (d) GRPL > 25.4375 kg m^{-2} between the future (2071–2100) and control (1971–2000) periods. (e) The average of these three grids. Grid boxes are 0.25° latitude × 0.275° longitude.

these larger magnitude events (Childs and Schumacher 2019); these percentages are applied to all event classes and are thus independent of magnitude.

5. Assessment of human exposure

a. Base case scenario

Base case MC simulations are run for both tornadoes and hail using the year-2000 GPW cost surface. Tornado and hail events are simulated over 1000 years, and their respective attributes and human exposure are calculated (Table 3). The simulated tornado tracks and hail density for the base case (Fig. 9) affirms the influence of the CTRL weighting surfaces (Figs. 5a,b) on the location of the selected reports. The average of 39 tornadoes per year and 247.5 severe hail events per year simulated by TorMC and HailMC, respectively, are very close to the actual 1997–2017 means from the SPC datasets (39.0 and 250.6, respectively) and thus capture the current probability. The mean magnitude of tornado events is 0.18, corresponding to an EF0 rating and reflecting the propensity for weak tornadoes across the domain. The average length, width, and azimuth angle are 1.66 km, 35.9 m, and 56.3° (northeastward), respectively, and the base case average hailstone size is 1.38 in. (35.1 mm). These statistics do not vary significantly with each new simulation. An average of 34.8 people are within the path of each simulated tornado and 30.2 people are within each hail swath, amounting to a mean of 1358 and 7474 and median of 1156 and 1334 persons per year, respectively. The rest of the cases are concerned

TABLE 3. Mean tornado and severe hail attributes and human exposure statistics from the base case 1000-yr MC simulations.

Statistic	Tornado	Hail
Annual count	39.0	247.5
Magnitude	EF0.18	1.38 in.
Pathlength	1.66 km	0.5 km
Path width	35.9 m	0.5 km
Azimuth	56.4°	0°
Human exposure	34.8	30.2
Annual human exposure	1358	7474

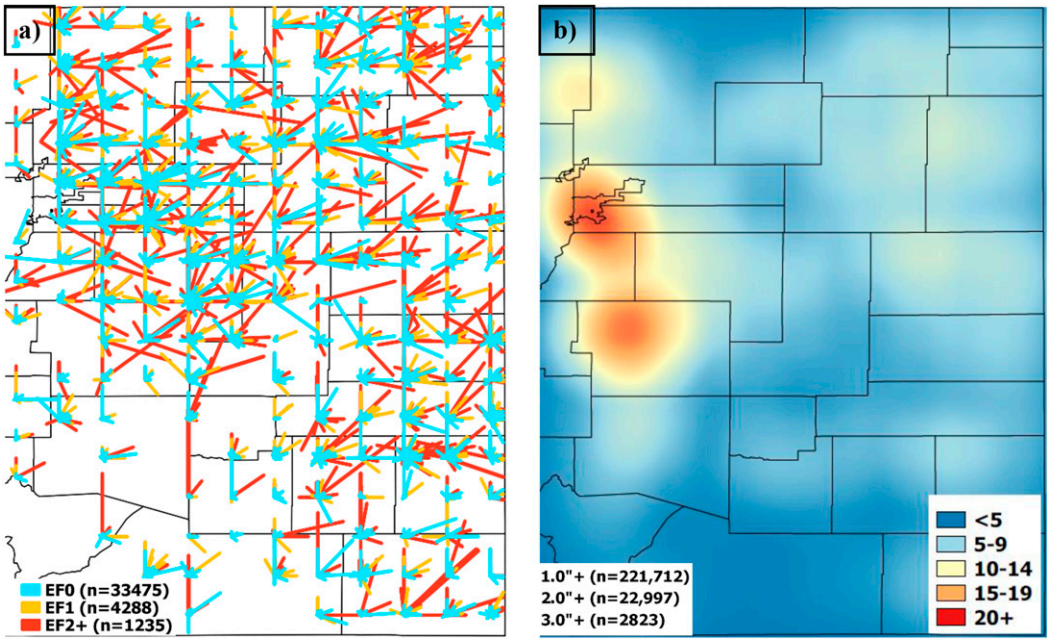

FIG. 9. (a) Simulated tornado tracks, partitioned by EF-scale intensity, and (b) heat map of simulated severe hail swaths using kernel density estimation, where the reddest shading represents in excess of 20 reports per year, for the base case scenarios within TorMC and HailMC.

with the relative change in either hazard occurrence or human exposure out to 2100, and thus actual numbers of tornadoes, hail events, and people exposed will not be shown. To isolate the individual impacts from population, spatial density of reports, and annual frequency, series of MC simulations are run holding constant one of these variables and adjusting the others based on projected changes.

b. Climatological contribution to human exposure

The first set of modified MC simulations explores the relative change in end-of-century hazard by increasing the annual frequency of tornadoes by 2.9% and severe hail by 3.5% uniformly over the domain. Simulations are conducted with both the CTRL and FUT weighting surfaces, while the base case GPW population cost surface is held constant, representing a theoretical future where no population or built-environment changes would occur. In these scenarios, mean annual counts increase by at least 2.2% for tornadoes and 3.8% for severe hail (Table 4), consistent with the projected amplification in frequency applied to the MC models. The slight differences in percent increase are due to the random nature of the MC simulation and not the spatial weighting surface.

Of greater interest is how changes in the climatological probability and spatial distribution of hazard occurrence independent of population (Tables 5 and 6, top block of rows) affects the human risk by changing number of people exposed to each hazard relative to the base case. In these scenarios, exposure (and thus risk) changes only via a geographical shift in hazard occurrence. First, a uniform percent increase in tornado and hail hazard applied to the CTRL spatial weighting surface results in 6.2% and 6.3% greater mean annual human exposure by the end of the century, as hazards are still preferentially selected by the MC models primarily in densely populated areas. However, increasing the hazard and applying the FUT weighting surface decreases mean annual human exposure by 14.6% for tornadoes and 75.7% for severe hail. This is attributed to the FUT weighting surface shifting the greatest tornado and hail probabilities toward eastern Colorado where population density is low. Thus, tornado and hail risk under these scenarios depends on the overlap of exposure (due the different weighting surfaces) and uniform hazard frequency.

c. Population contribution to human exposure

This section controls for any potential future changes in tornado and hail environments while allowing future population to evolve throughout eastern Colorado (Tables 5 and 6, second block of rows). All population growth scenarios except SSP3 lead to a substantial increase in human exposure. Although a range of potential changes is revealed, the SSP5 produces a 154.6% increase in

TABLE 4. Annual tornado and severe hail statistics for scenarios with constant base case population cost surface.

Scenario			Annual statistics				
Cost surface	Frequency	Spatial weighting	Mean	Change in mean	Max	Median	Std dev
				Tornado statistics			
Base case	Control	Control	39.0	—	78	37	16.8
Base case	+2.9%	Control	39.8	+2.2%	80	38	17.4
Base case	+2.9%	Future	40.2	+3.1%	80	38	16.6
				Severe hail statistics			
Base case	Control	Control	247.5	-	468	213	100
Base case	+3.5%	Control	259.2	+4.7%	484	220	107
Base case	+3.5%	Future	257.0	+3.8%	484	220	102

tornado exposure and a 161.0% escalation in severe hail exposure. Conversely, the SSP3 reduces mean annual human exposure to tornadoes by 8.4% and slightly increases human exposure to severe hail by 0.1%. To recall, SSP5 produces widespread population growth across eastern Colorado, particularly along the urban corridor, and SSP3 produces only small pockets of growth in metropolitan areas alongside areas of decreasing population; hence the spread in potential end-of-century human exposure. Comparing these statistics with those in Table 4, where population is held constant, it is apparent that changes in population (except the SSP3 scenario) exert a greater influence on human exposure than climatological changes in tornado and severe hail landscapes. This result agrees qualitatively with Strader et al. (2017), who found that changes in the number of housing units outweighed changes in tornado occurrence toward increasing overall risk.

d. *Mutual contribution to human exposure*

Two series of simulations are employed to investigate the mutual contribution of climatological and population changes on end-of-century human exposure. In the first set of simulations (Tables 5 and 6, third block of rows), each SSP surface is overlaid on top of tornado and severe hail surfaces that have been generated by altering the frequency of these hazards but retaining the CTRL hazard spatial distribution. Escalating the frequency of tornadoes is not sufficient to overcome the decreasing population patterns in SSP3, resulting in a smaller human exposure compared to the base case. For all other

TABLE 5. Annual human exposure to tornadoes across eastern Colorado. Different cases are simulated by varying the cost surface of SSP population scenarios, the frequency of tornadoes as projected by the WRF analysis, and the spatial probability surface of either historical data or the projected synthetic reports distributions. Aside from the percent change in the annual mean, the units shown are number of people.

Scenario			Annual human exposure				
Cost surface	Frequency	Spatial weighting	Mean	Change in mean	Max	Median	Std dev
Base case	Control	Control	1358	—	25 991	449	3056
Base case	+2.9%	Control	1442	+6.2%	79 663	428	4516
Base case	+2.9%	Future	1159	−14.6%	61 011	332	3735
SSP1	Control	Control	2240	+65.0%	47 624	583	5590
SSP2	Control	Control	2201	+62.1%	46 864	569	5503
SSP3	Control	Control	1244	−8.4%	27 330	285	3220
SSP4	Control	Control	1742	+28.3%	37 558	431	4418
SSP5	Control	Control	3457	+154.6%	71 277	989	8348
SSP1	+2.9%	Control	2413	+77.7%	147 176	543	8324
SSP2	+2.9%	Control	2371	+74.6%	144 890	529	8195
SSP3	+2.9%	Control	1347	−0.8%	84 888	259	4805
SSP4	+2.9%	Control	1881	+38.5%	116 373	393	6585
SSP5	+2.9%	Control	3707	+173.0%	219 367	930	12 396
SSP1	+2.9%	Future	1914	+40.9%	113 001	427	6865
SSP2	+2.9%	Future	1881	+38.5%	111 256	417	6760
SSP3	+2.9%	Future	1067	−21.4%	65 187	210	3960
SSP4	+2.9%	Future	1491	+9.8%	89 353	315	5429
SSP5	+2.9%	Future	2943	+116.7%	168 411	720	10 234

TABLE 6. As in Table 5, but for annual human exposure to severe hailstorms.

Scenario			Annual human exposure				
Cost surface	Frequency	Spatial weighting	Mean	Change in mean	Max	Median	Std dev
Base case	Control	Control	7474	—	20 979	6746	3539
Base case	+3.5%	Control	7947	+6.3%	22 956	7201	3849
Base case	+3.5%	Future	1816	−75.7%	6769	1587	1053
SSP1	Control	Control	13 028	+74.3%	37 180	11 718	6251
SSP2	Control	Control	12 827	+71.6%	36 622	11 539	6156
SSP3	Control	Control	7485	+0.1%	21 494	6731	3610
SSP4	Control	Control	10 297	+37.8%	29 468	9254	4952
SSP5	Control	Control	19 509	+161.0%	55 355	17 574	9315
SSP1	+3.5%	Control	13 858	+85.4%	40 665	12 589	6087
SSP2	+3.5%	Control	13 646	+82.6%	40 053	12 398	6705
SSP3	+3.5%	Control	7964	+6.6%	23 496	7260	3933
SSP4	+3.5%	Control	10 955	+46.6%	32 221	9972	5394
SSP5	+3.5%	Control	20 749	+177.6%	60 569	18 829	10 141
SSP1	+3.5%	Future	2877	−61.5%	11 384	2498	1794
SSP2	+3.5%	Future	2825	−62.2%	11 196	2452	1765
SSP3	+3.5%	Future	1590	−78.7%	6451	1382	1024
SSP4	+3.5%	Future	2234	−70.1%	8941	1940	1413
SSP5	+3.5%	Future	4459	−40.3%	17 263	3899	2705

SSPs, human exposure increases slightly over the changing-population-constant-risk scenarios and by as much as 173.0% over the base case. When both frequency and spatial distribution of tornadoes are modified (Table 5, bottom block of rows), the resulting change in human exposure is lower for each SSP relative to solely changing the tornado frequency. Nevertheless, each SSP aside from SSP3 (−21.4%) still yields an appreciable amplification in human exposure relative to the base case.

Raising the probability of severe hail over the domain (Table 6, third block of rows), in addition to population changes, results in a greater mean annual human exposure by as much as 177.6% over the base case scenario. In fact, all SSPs yield a quantitatively larger increase in human exposure compared to when the future hail frequency is applied to the base case scenario, once again affirming a strong population influence on the number of persons exposed to the hazard. When all factors are allowed to change, a decrease in human exposure is predicted for each SSP relative to the base case scenario, from −40.3% for SSP5 to −78.7% for SSP3 (Table 6, bottom block of rows). The eastward shift of the largest frequencies of severe hail in the future into less populated areas is responsible for this reduction.

6. Discussion and implications

Understanding potential future changes in both population and tornado/severe hail landscapes is crucial to forecasting future human risk and the associated impacts. Eastern Colorado in particular, presents a unique region for this work. Not only does this region have one of the fastest growing metropolitan areas alongside an extensive rural area, but it also represents one of the most active tornado and severe hail regions of the United States. That said, the methods presented herein may be applied to other regions across the United States to reveal other local trends in both meteorological and nonmeteorological variables that can influence local severe weather risk.

The projected population distributions and hazard landscapes across eastern Colorado present a wide range of potential end-of-century tornado and hail exposure outcomes based on the MC results presented in this study. Examining future tornado and hail events, the synthetic reports approach predicts only a marginal increase in the number of tornado and severe hail days across eastern Colorado by 2100. This base case future tornado and hail scenario results in only modest increases in human exposure to these hazards. If the hazards were to increase above projected levels within eastern Colorado, higher risks will result. Assuming the current means of 2.5 tornado reports and 5.9 hail reports per tornado and hail day, respectively, remains constant, up to 2.5 additional tornado and 18 additional hail reports per year can be expected in those grid boxes with the greatest frequency of tornadoes or hail. These findings are in line with Childs and Schumacher (2019), who reported increasing trends in severe hail reports and hail days at all size thresholds within the eastern Colorado region since 1997, and Trapp et al. (2019) who showed projected future increases in large hail frequency over this region using dynamical downscaling techniques.

Together, these studies suggest that if the future hail event scenarios are realized, not only could more hail be reported in northeastern Colorado, but a greater number of significant hailstones could also fall on more days.

In general, most parameters used as proxies for tornado and severe hail events indicate a future increase in frequency domainwide, maximized in northeastern Colorado. However, this eastward shift leads to decreasing human exposure to severe hail relative to the base case scenario and a smaller increase in exposure to tornadoes relative to scenarios that use the CTRL spatial distribution. Changing the spatial distribution of hazards according to projections from high-resolution weather model output is unique to this study, as previous work by Strader et al. (2017) experimented with the same change in frequency over their entire domain of interest. Along the Front Range urban corridor, the number of tornado and severe hail days are also projected to increase, just not as much. Thus, one would still expect to see an escalating number of tornado and hail reports in these populated areas. In particular, areas east of downtown Denver have experienced significant growth in the past 5 years, as hotels, restaurants, and a major resort have strategically moved into the area to serve as a gateway to the airport. It is inevitable that housing will continue to expand into this area as well, which will not only add to the built environment but also put people into a zone of enhanced tornado and hail risk. In addition, the SSP1, SSP2, and SSP5 scenarios show appreciable growth around Fort Morgan in northeastern Colorado, which is within the maximum projected increase in both tornado and severe hail occurrence; if population does indeed grow in this area, there would be a need to raise public awareness of the heightened risk from these hazards.

The eastward shift in projected severe hail frequency, though producing decreased human exposure, does result in a greater number of hailstorms affecting agricultural land. Crop losses from hailstorms not only reduces yields but also places stresses on the market, as some $41 billion is contributed from the agricultural sector to the Colorado economy each year (Colorado State University 2012). Recent high-resolution land-use projections across the Great Plains from the U.S. Geological Survey (Sohl et al. 2018) can be used to support this hypothesized projected rise in agricultural exposure. Inputting their base case (year 2014) land-use surface for a ''business as usual'' climate scenario, clipped to the eastern Colorado domain, into HailMC results in a 14% increase in the amount of agricultural land exposed to hailstorms on any given year by the end of this century using the FUT hail weighting surface. Future work is warranted to assess how changes in agricultural land-use patterns may impact crop exposure to severe weather hazards. Toward this end, an interview study was conducted in summer 2019 with eastern Colorado agriculturalists by the first author, with the goal of increasing awareness of the needs and vulnerabilities of the agrarian population toward severe hailstorms (Childs et al. 2020, manuscript submitted to *Wea. Climate Soc.*). This work becomes even more important in light of the MC results presented here.

While population growth and urban expansion are likely to continue, there are steps that can be taken as people continue to move into areas that are projected to be at greater risk from tornadoes and hailstorms in the future. Arguably of first priority is increasing public awareness, which must be wrought with intentional and planned endeavors. Especially in largely rural areas like eastern Colorado, risk communication faces numerous challenges. People moving into the state from elsewhere for business, retirement, or recreation purposes may be unaware that Colorado is in fact a state prone to tornadoes and damaging hailstorms since it is not in the traditional ''Tornado Alley'' or the Southeast. Thus, newcomers must be made aware of the risk so they can make informed decisions about living location, types and amount of insurance to buy, and protective measures to take. It is through the synthesis of research and communication that the local public can be informed of the changing risk from severe weather and the negative impacts of such hazards can be mitigated.

7. Conclusions

This study offers a first look at how population and meteorology work separately and together to modify human exposure by the end of the twenty-first century across the localized domain of eastern Colorado. A wide range of potential changes in the number of people exposed to these hazards is revealed. Two MC models are utilized that repeatedly sample tornado and severe hail events according to spatial probabilities of these hazards over eastern Colorado in a current and future climate. Projections of severe weather hazards out to the year 2100 have been made through a synthetic reports approach, wherein convective parameters serving as proxies for tornado and severe hail reports are compared between two high-resolution WRF simulations of current and future climate scenarios (Hoogewind et al. 2017). This analysis predicts a domainwide increase in the average annual tornado and severe hail days by the end of this century, with up to one more day of tornadoes and three more days of severe hail per year by this time. Maximum increases in both

hazards are concentrated in an arc across northeastern Colorado with subtle yet noteworthy differences.

Population projections out to 2100 are taken from the SSPs and cropped to the eastern Colorado domain. Most SSPs project increasing population along the Front Range urban corridor with lesser change farther east, but key differences exist in both magnitude and spatial patterns that influence the number of people potentially exposed to the severe weather hazards. MC simulations are run for 1000 years and reveal that future human exposure is highly dependent upon population dynamics and the spatial distribution of hazards, particularly for hail. Alternating population scenarios in constant hazard results in a broad spectrum of changes in end-of-century annual mean human exposure, ranging from −8.4% to +154.6% for tornadoes and from +0.1% to +161.0% for severe hail. The largest magnitude of increase in projected human exposure for both hazards occurs when population and frequency of the hazard changes but the spatial distribution is held at the historical state. Under this scenario, a 177.6% increase in human exposure to severe hail is predicted by 2100. When spatial distribution of tornado and hail hazards are incorporated, a decline in human exposure is projected. This affirms the sensitivity of the human system to changes in meteorology; despite climate change signals, the amount of risk actually has the potential to decrease in local contexts due to the overlapping effect of meteorological and population changes. The implications of this sensitivity on policy makers is important, as determination of future risk for local communities and the associated mitigation strategies must consider these distinct possibilities.

This study acknowledges a wide range of uncertainty with exactly how many people in eastern Colorado will be exposed to tornadoes and severe hail in the future, and it is not of interest to predict which scenario is the most probable. While it is reasonable to posit continued population growth and eastward expansion of the Front Range urban corridor, many factors, some unforeseen, could influence future population distribution within the domain. Further, the synthetic reports approach taken here is one of a variety of potential methods to project frequency and spatial distributions of tornadoes and severe hail. This study also cannot completely avoid the population bias inherent in the SPC severe weather database, although the use of tornado and severe hail days as the measure of hazard frequency and convective parameters as proxies for reports can better capture the changing distribution of favorable severe weather predictors. It should also be mentioned that an increasing human exposure does not necessarily mean increasing human injuries, fatalities, or property losses.

The hope is that increasing awareness of potential changes in exposure, the continued technological advancements in long- and short-term severe weather forecasting, and improved mitigation strategies by a wide variety of local sectors can help avert more serious human and property impacts. For example, land-use and urban planners can develop growth strategies in light of the changing severe weather landscape. New building construction and the associated codes should address the evolving hazard risk, particularly for severe hail, as strong building codes have shown promise in reducing hail risk (Czajkowski and Simmons 2014). Relatedly, vulnerable entities such as automobile dealerships and recreation areas in Colorado that have suffered extensive damage from hailstorms in recent years have taken steps toward hazard mitigation (CBS4 Denver 2019; Reid 2019). In light of the projected amplified hazard probabilities in rural areas of the eastern plains, agricultural interests should work to implement alternative crops that are more resilient to severe weather impacts, knowing that crop insurance, although arguably the most effective mitigative strategy for farmers, is not an end-all solution. In fact, this study motivated a series of interviews with eastern Colorado farmers and ranchers to gauge their perceptions of severe hail vulnerability, risk factors, and mitigation strategies (Childs et al. 2020, manuscript submitted to *Wea. Climate Soc.*). It is also imperative that assessment of changing hazard risk and exposure be communicated to the local population in a comprehensible manner. Meteorologists play a critical role in providing this effective communication and can also benefit from projections of future human exposure as they work to continue advancements in tornado and hailstorm predictability. Given the wide range of potential changes in human exposure, and in turn the human risk, residents of eastern Colorado are encouraged to take steps now to prepare for future tornadoes and hailstorms.

Acknowledgments. The authors are especially grateful to Dr. Kim Hoogewind for sharing the WRF data and helping with interpretation. Drs. Kristen Rasmussen, Ryan Sobash, and Brian O'Neill also provided helpful feedback on various aspects of the methods. The authors are thankful for three reviewers who provided helpful comments toward improving the paper. This work is made possible through funding from the National Science Foundation (NSF) Graduate Research Fellowship Program Grant DGE-1321845 as well as NSF Grant AGS-1637244.

REFERENCES

Agee, E. M., and S. J. Childs, 2014: Adjustments in tornado counts, F-scale intensity, and path width for assessing significant tornado destruction. *J. Appl. Meteor. Climatol.*, **53**, 1494–1505, https://doi.org/10.1175/JAMC-D-13-0235.1.

Allen, J. T., and M. K. Tippett, 2015: The characteristics of United States hail reports: 1955–2014. *Electron. J. Severe Storms Meteor.*, **10** (3), http://www.ejssm.org/ojs/index.php/ejssm/article/viewArticle/149.

——, ——, and A. H. Sobel, 2015a: An empirical model relating us monthly hail occurrence to large-scale meteorological environment. *J. Adv. Model. Earth Syst.*, **7**, 226–243, https://doi.org/10.1002/2014MS000397.

——, ——, and ——, 2015b: Influence of the El Niño/Southern Oscillation on tornado and hail frequency in the United States. *Nat. Geosci.*, **8**, 278–283, https://doi.org/10.1038/ngeo2385.

Ashley, W. S., 2007: Spatial and temporal analysis of tornado fatalities in the United States: 1880–2005. *Wea. Forecasting*, **22**, 1214–1228, https://doi.org/10.1175/2007WAF2007004.1.

——, and S. M. Strader, 2016: Recipe for disaster: How the dynamic ingredients of risk and exposure are changing the tornado disaster landscape. *Bull. Amer. Meteor. Soc.*, **97**, 767–786, https://doi.org/10.1175/BAMS-D-15-00150.1.

——, ——, T. Rosencrants, and A. J. Krmenec, 2014: Spatiotemporal changes in tornado hazard exposure: The case of the expanding bull's-eye effect in Chicago, Illinois. *Wea. Climate Soc.*, **6**, 175–193, https://doi.org/10.1175/WCAS-D-13-00047.1.

Barker, H. W., R. K. Goldstein, and D. E. Stevens, 2003: Monte Carlo simulation of solar reflectances for cloudy atmospheres. *J. Atmos. Sci.*, **60**, 1881–1894, https://doi.org/10.1175/1520-0469(2003)060<1881:MCSOSR>2.0.CO;2.

Bouwer, L. M., 2011: Have disaster losses increased due to anthropogenic climate change? *Bull. Amer. Meteor. Soc.*, **92**, 39–46, https://doi.org/10.1175/2010BAMS3092.1.

——, 2013: Projections of future extreme weather losses under changes in climate and exposure. *Risk Anal.*, **33**, 915–930, https://doi.org/10.1111/j.1539-6924.2012.01880.x.

——, 2019: Observed and projected impacts from extreme weather events: Implications for loss and damage. *Loss and Damage from Climate Change*, Springer, 63–82.

Brady, R. H., and E. J. Szoke, 1989: A case study of nonmesocyclone tornado development in northeast Colorado: Similarities to waterspout formation. *Mon. Wea. Rev.*, **117**, 843–856, https://doi.org/10.1175/1520-0493(1989)117<0843:ACSONT>2.0.CO;2.

Brimelow, J. C., W. R. Burrows, and J. M. Hanesiak, 2017: The changing hail threat over North American in response to anthropogenic climate change. *Nat. Climate Change*, **7**, 516–522, https://doi.org/10.1038/nclimate3321.

Brooks, H. E., 2004: On the relationship of tornado path length and width to intensity. *Wea. Forecasting*, **19**, 310–319, https://doi.org/10.1175/1520-0434(2004)019<0310:OTROTP>2.0.CO;2.

——, 2009: Proximity soundings for severe convection for Europe and the United States from reanalysis data. *Atmos. Res.*, **93**, 546–553, https://doi.org/10.1016/j.atmosres.2008.10.005.

——, 2013: Severe thunderstorms and climate change. *Atmos. Res.*, **123**, 129–138, https://doi.org/10.1016/j.atmosres.2012.04.002.

——, C. A. Doswell III, and M. P. Kay, 2003a: Climatological estimates of local daily tornado probability for the United States. *Wea. Forecasting*, **18**, 626–640, https://doi.org/10.1175/1520-0434(2003)018<0626:CEOLDT>2.0.CO;2.

——, J. W. Lee, and J. P. Craven, 2003b: The spatial distribution of severe thunderstorm and tornado environments from global reanalysis data. *Atmos. Res.*, **67–68**, 73–94, https://doi.org/10.1016/S0169-8095(03)00045-0.

CBS4 Denver, 2019: Cheyenne Mountain Zoo rebuilds after devastating hail storm. Accessed 3 March 2020, https://denver.cbslocal.com/2019/01/25/cheyenne-mountain-zoo-hail-storm-colorado-springs/.

Center for International Earth Science Information Network, 2011: Global Rural-Urban Mapping Project (GRUMP), version 1. NASA Socioeconomic Data and Applications Center, accessed 20 May 2019, http://sedac.ciesin.columbia.edu/data/collection/grump-v1.

Changnon, S. A., 1999: Data and approaches for determining hail risk in the contiguous United States. *J. Appl. Meteor.*, **38**, 1730–1739, https://doi.org/10.1175/1520-0450(1999)038<1730:DAAFDH>2.0.CO;2.

——, 2009: Increasing major hail losses in the U.S. *Climatic Change*, **96**, 161–166, https://doi.org/10.1007/s10584-009-9597-z.

——, R. Pielke Jr., D. Changnon, R. Sylves, and R. Pulwarty, 2000: Human factors explain the increased losses from weather and climate extremes. *Bull. Amer. Meteor. Soc.*, **81**, 437–442, https://doi.org/10.1175/1520-0477(2000)081<0437:HFETIL>2.3.CO;2.

Chen, J., A. Dai, Y. Zhang, and K. L. Rasmussen, 2020: Changes in convective available potential energy and convective inhibition under global warming. *J. Climate*, **33**, 2025–2050, https://doi.org/10.1175/JCLI-D-19-0461.1.

Childs, S. J., and R. S. Schumacher, 2018a: Cold-season tornado risk communication: Case studies from November 2016 to February 2017. *Wea. Climate Soc.*, **10**, 419–433, https://doi.org/10.1175/WCAS-D-17-0073.1.

——, and ——, 2018b: The anomalously large 2018 hail season of eastern Colorado: A local perspective on a national trend. *29th Conf. on Severe Local Storms*, Stowe, VT, Amer. Meteor. Soc., **33**, https://ams.confex.com/ams/29SLS/webprogram/Paper348238.html.

——, and ——, 2019: An updated severe hail and tornado climatology for eastern Colorado. *J. Appl. Meteor. Climatol.*, **58**, 2273–2293, https://doi.org/10.1175/JAMC-D-19-0098.1.

Cintineo, J. L., T. M. Smith, V. Lakshmanan, H. E. Brooks, and K. L. Ortega, 2012: An objective high-resolution hail climatology of the contiguous United States. *Wea. Forecasting*, **27**, 1235–1248, https://doi.org/10.1175/WAF-D-11-00151.1.

Clark, A. J., J. Gao, P. T. Marsh, T. Smith, J. S. Kain, J. Correia, M. Xue, and F. Kong, 2013: Tornado pathlength forecasts from 2010 to 2011 using ensemble updraft helicity. *Wea. Forecasting*, **28**, 387–407, https://doi.org/10.1175/WAF-D-12-00038.1.

——, J. S. Kain, P. T. Marsh, J. Correia Jr., M. Xue, and F. Kong, 2012: Forecasting tornado pathlengths using a three-dimensional object identification algorithm applied to convection-allowing forecasts. *Wea. Forecasting*, **27**, 1090–1113, https://doi.org/10.1175/WAF-D-11-00147.1.

Colorado State Demography Office, 2012: Projected population change: 2010 to 2040. CSDO, https://storage.googleapis.com/maps-static/TotalPopChange2010_2040.pdf.

Colorado State University, 2012: The contribution of agriculture to Colorado's economy: An executive summary—January 2012. State of Colorado, https://www.colorado.gov/pacific/sites/default/files/CSU%20Executive%20Summary.pdf.

Creighton, G., E. Kuchera, R. Adams-Selin, J. McCormick, S. Rentschler, and B. Wickard, 2014: AFWA diagnostics in WRF. Air Force Weather Agency, 2nd Weather Group Doc., 17 pp., https://www2.mmm.ucar.edu/wrf/users/docs/AFWA_Diagnostics_in_WRF.pdf.

Cutter, S. L., J. T. Mitchell, and M. S. Scott, 2000: Revealing the vulnerability of people and places: A case study of Georgetown County, South Carolina. *Ann. Assoc. Amer. Geogr.*, **90**, 713–737, https://doi.org/10.1111/0004-5608.00219.

Czajkowski, J., and K. M. Simmons, 2014: Convective storm vulnerability: Quantifying the role of effective and well-enforced building codes in minimizing Missouri hail property damage. *Land Econ.*, **90**, 482–508, https://doi.org/10.3368/le.90.3.482.

Dessens, J., C. Berthet, and J. L. Sanchez, 2015: Change in hailstone size distributions with an increase in the melting level height. *Atmos. Res.*, **158–159**, 245–253, https://doi.org/10.1016/j.atmosres.2014.07.004.

Diffenbaugh, N. S., M. Scherer, and R. J. Trapp, 2013: Robust increases in severe thunderstorm environments in response to greenhouse forcing. *Proc. Natl. Acad. Sci. USA*, **110**, 16 361–16 366, https://doi.org/10.1073/pnas.1307758110.

Donner, L. J., and Coauthors, 2011: The dynamical core, physical parameterizations, and basic simulation characteristics of the atmospheric component AM3 of the GFDL global coupled model CM3. *J. Climate*, **24**, 3484–3519, https://doi.org/10.1175/2011JCLI3955.1.

Doswell, C. A., 1980: Synoptic-scale environments associated with high plains severe thunderstorms. *Bull. Amer. Meteor. Soc.*, **61**, 1388–1400, https://doi.org/10.1175/1520-0477(1980)061<1388:SSEAWH>2.0.CO;2.

Ebi, K. L., and Coauthors, 2014: A new scenario framework for climate change research: Background, process, and future directions. *Climatic Change*, **122**, 363–372, https://doi.org/10.1007/s10584-013-0912-3.

Edwards, R., and R. L. Thompson, 1998: Nationwide comparisons of hail size with WSR-88D vertically integrated liquid water and derived sounding data. *Wea. Forecasting*, **13**, 277–285, https://doi.org/10.1175/1520-0434(1998)013<0277:NCOHSW>2.0.CO;2.

Farney, T. J., and P. G. Dixon, 2015: Variability of tornado climatology across the continental United States. *Int. J. Climatol.*, **35**, 2993–3006, https://doi.org/10.1002/joc.4188.

Gagne, D. J., A. McGovern, S. E. Haupt, R. A. Sobash, J. K. Williams, and M. Xue, 2017: Storm-based probabilistic hail forecasting with machine learning applied to convection-allowing ensembles. *Wea. Forecasting*, **32**, 1819–1840, https://doi.org/10.1175/WAF-D-17-0010.1.

Gallo, B. T., A. J. Clark, and S. R. Dembek, 2016: Forecasting tornadoes using convection-permitting ensembles. *Wea. Forecasting*, **31**, 273–295, https://doi.org/10.1175/WAF-D-15-0134.1.

——, and Coauthors, 2017: Breaking new ground in severe weather prediction: The 2015 NOAA/Hazardous Weather Testbed spring forecasting experiment. *Wea. Forecasting*, **32**, 1541–1568, https://doi.org/10.1175/WAF-D-16-0178.1.

Gao, J., 2017: Downscaling global spatial population projections from 1/8-degree to 1-km grid cells. NCAR Tech. Note NCAR/TN-537+STR, 14 pp., https://doi.org/10.5065/D60Z721H.

Gensini, V. A., and T. L. Mote, 2014: Estimations of hazardous convective weather in the United States using dynamical downscaling. *J. Climate*, **27**, 6581–6589, https://doi.org/10.1175/JCLI-D-13-00777.1.

——, and ——, 2015: Downscaled estimates of late 21st century severe weather from CCSM3. *Climatic Change*, **129**, 307–321, https://doi.org/10.1007/s10584-014-1320-z.

——, and H. E. Brooks, 2018: Spatial trends in United States tornado frequency. *npj Climate Atmos. Sci.*, **1**, 38, https://doi.org/10.1038/s41612-018-0048-2.

Hoogewind, K. A., M. E. Baldwin, and R. J. Trapp, 2017: The impact of climate change on hazardous convective weather in the United States: Insight from high-resolution dynamical downscaling. *J. Climate*, **30**, 10 081–10 100, https://doi.org/10.1175/JCLI-D-16-0885.1.

IPCC, 2012: *Managing the Risks of Extreme Events and Disasters to Advance Climate Change Adaptation*. Cambridge University Press, 582 pp., https://www.ipcc.ch/site/assets/uploads/2018/03/SREX_Full_Report-1.pdf.

Jones, B., and B. C. O'Neill, 2013: Historically grounded spatial population projections for the continental United States. *Environ. Res. Lett.*, **8**, 044021, https://doi.org/10.1088/1748-9326/8/4/044021.

——, and ——, 2016: Spatially explicit global population scenarios consistent with the Shared Socioeconomic Pathways. *Environ. Res. Lett.*, **11**, 084003, https://doi.org/10.1088/1748-9326/11/8/084003.

Kain, J. S., and Coauthors, 2008: Some practical considerations regarding horizontal resolution in the first generation of operational convection-allowing NWP. *Wea. Forecasting*, **23**, 931–952, https://doi.org/10.1175/WAF2007106.1.

Maddox, R., D. Rodgers, W. Deitrich, and D. Bartels, 1981: Meteorological settings associated with significant convective storms in Colorado. NOAA Tech. Memo ERL OWRM-4, 75 pp.

Mahoney, K., M. A. Alexander, G. Thompson, J. J. Barsugli, and J. D. Scott, 2012: Changes in hail and flood risk in high-resolution simulations over Colorado's mountains. *Nat. Climate Change*, **2**, 125–131, https://doi.org/10.1038/nclimate1344.

Martius, O., A. Hering, M. Kunz, A. Manzato, S. Mohr, L. Nisi, and S. Trefalt, 2018: Challenges and recent advances in hail research. *Bull. Amer. Meteor. Soc.*, **99**, ES51–ES54, https://doi.org/10.1175/BAMS-D-17-0207.1.

Martynov, A., L. Nisi, and O. Martius, 2017: Summertime hailstorms over Switzerland in 2012–2015 in convection-permitting WRF simulations: Assessment of modeling performance. *Geophysical Research Abstracts*, Vol. 19, Abstract 7501, https://meetingorganizer.copernicus.org/EGU2017/EGU2017-7501.pdf.

Mooney, C. Z., 1997: *Monte Carlo Simulation*. Sage Publications, 103 pp.

Morss, R. E., O. V. Wilhelmi, G. A. Meehl, and L. Dilling, 2011: Improving societal outcomes of extreme weather in a changing climate: An integrated perspective. *Annu. Rev. Environ. Resour.*, **36**, 1–25, https://doi.org/10.1146/annurev-environ-060809-100145.

——, K. J. Mulder, J. K. Lazo, and J. L. Demuth, 2016: How do people perceive, understand, and anticipate responding to flash flood risks and warnings? Results from a public survey in Boulder, Colorado, USA. *J. Hydrol.*, **541**, 649–664, https://doi.org/10.1016/j.jhydrol.2015.11.047.

Nagele, D. E., and J. E. Trainor, 2012: Geographic specificity, tornadoes, and protective action. *Wea. Climate Soc.*, **4**, 145–155, https://doi.org/10.1175/WCAS-D-11-00047.1.

Nakićenović, N., and R. Swart, Eds., 2000: *IPCC Special Report on Emissions Scenarios*. Cambridge University Press, 570 pp.

National Research Council, 2009: *Science and Decisions: Advancing Risk Assessment*. The National Academies Press, 422 pp.

O'Neill, B. C., E. Kriegler, K. Riahi, K. L. Ebi, S. Hallegatte, T. R. Carter, R. Mathur, and D. P. van Vuuren, 2013: A new scenario framework for climate change research: The concept of shared socioeconomic pathways. *Climatic Change*, **122**, 387–400, https://doi.org/10.1007/s10584-013-0905-2.

Paul, B. K., 2011: *Environmental Hazards: Contexts, Perspectives and Management*. John Wiley and Sons, 334 pp.

Pielke, R., Jr., and E. Mills, 2005: Attribution of disaster losses. *Science*, **310**, 1615–1616, https://doi.org/10.1126/science.310.5754.1615c.

Potvin, C. K., C. Broyles, P. S. Skinner, H. E. Brooks, and E. Rasmussen, 2019: A Bayesian hierarchical modeling framework for correcting reporting bias in the US tornado database. *Wea. Forecasting*, **34**, 15–30, https://doi.org/10.1175/WAF-D-18-0137.1.

Prein, A. F., and G. J. Holland, 2018: Global estimates of damaging hail hazard. *Wea. Climate Extremes*, **22**, 10–23, https://doi.org/10.1016/j.wace.2018.10.004.

Rasmussen, R., and H. R. Pruppacher, 1982: A wind tunnel and theoretical study of the melting behavior of atmospheric ice particles. I: A wind tunnel study of frozen drops of radius $< 500\ \mu$m. *J. Atmos. Sci.*, **39**, 152–158, https://doi.org/10.1175/1520-0469(1982)039<0152:AWTATS>2.0.CO;2.

Rasmussen, K. L., A. F. Prein, R. M. Rasmussen, K. Ikeda, and C. Liu, 2020: Changes in the convective population and thermodynamic environments in convection-permitting regional climate simulations over the United States. *Climate Dyn.*, https://doi.org/10.1007/s00382-017-4000-7, in press.

Reid, T., 2019: Ehrlich Toyota planning solar carport to mitigate hail damage, generate power. *Greeley Tribune*, 11 March 2019, accessed 3 March 2020, https://www.greeleytribune.com/news/ehrlich-toyota-planning-solar-carport-to-mitigate-hail-damage-generate-power/.

Robinson, E. D., R. J. Trapp, and M. E. Baldwin, 2013: The geospatial and temporal distributions of severe thunderstorms from high-resolution dynamical downscaling. *J. Appl. Meteor. Climatol.*, **52**, 2147–2161, https://doi.org/10.1175/JAMC-D-12-0131.1.

Rocky Mountain Insurance Information Association, 2019: Hail damage and statistics. RMIIA, accessed 12 September 2019, http://www.rmiia.org/catastrophes_and_statistics/Hail.asp.

Rosencrants, T. D., and W. S. Ashley, 2015: Spatiotemporal analysis of tornado exposure in five US metropolitan areas. *Nat. Hazards*, **78**, 121–140, https://doi.org/10.1007/s11069-015-1704-z.

Samir, K. C., and W. Lutz, 2017: The human core of the shared socioeconomic pathways: Population scenarios by age, sex and level of education for all countries to 2100. *Global Environ. Change*, **42**, 181–192, https://doi.org/10.1016/j.gloenvcha.2014.06.004.

Schumacher, R., 2019: Colorado State record hailstone near Bethune. State Climate Extremes Committee Memo., 10 pp., https://www.ncdc.noaa.gov/monitoring-content/extremes/scec/reports/20191004-Colorado-Hailstone.pdf.

Seeley, J. T., and D. M. Romps, 2015: The effect of global warming on severe thunderstorms in the United States. *J. Climate*, **28**, 2443–2458, https://doi.org/10.1175/JCLI-D-14-00382.1.

Smith, A. B., 2019: 2018's billion dollar disasters in context. NOAA, https://www.climate.gov/news-features/blogs/beyond-data/2018s-billion-dollar-disasters-context.

——, and J. L. Matthews, 2015: Quantifying uncertainty and variable sensitivity within the US billion-dollar weather and climate disaster cost estimates. *Nat. Hazards*, **77**, 1829–1851, https://doi.org/10.1007/s11069-015-1678-x.

Sobash, R. A., 2018: Identifying severe convection in convection-permitting weather forecasts: State of the science and applications to convection-permitting climate simulations. Preprints, *Second GEWEX Convection-Permitting Climate Modeling Workshop*, Boulder, CO, NCAR, https://ral.ucar.edu/sites/default/files/public/events/2018/gewex-convection-permitting-climate-modeling-workshop-ii/docs/thursday-cpm-workshop.-sobash.pdf.

——, and J. S. Kain, 2017: Seasonal variations in severe weather forecast skill in an experimental convection-allowing model. *Wea. Forecasting*, **32**, 1885–1902, https://doi.org/10.1175/WAF-D-17-0043.1.

——, D. R. Bright, A. R. Dean, J. S. Kain, M. Coniglio, S. J. Weiss, and J. J. Levit, 2008: Severe storm forecast guidance based on explicit identification of convective phenomena in WRF-model forecasts. *24th Conf. on Severe Local Storms,* Savannah, GA, Amer. Meteor. Soc., 11.3, https://ams.confex.com/ams/24SLS/techprogram/paper_142187.htm.

——, J. S. Kain, D. R. Bright, A. R. Dean, M. C. Coniglio, and S. J. Weiss, 2011: Probabilistic forecast guidance for severe thunderstorms based on the identification of extreme phenomena in convection-allowing model forecasts. *Wea. Forecasting*, **26**, 714–728, https://doi.org/10.1175/WAF-D-10-05046.1.

——, C. S. Schwartz, G. S. Romine, K. R. Fossell, and M. L. Weisman, 2016: Severe weather prediction using storm surrogates from an ensemble forecasting system. *Wea. Forecasting*, **31**, 255–271, https://doi.org/10.1175/WAF-D-15-0138.1.

Sobel, A. H., and M. K. Tippett, 2018: Extreme events: Trends and risk assessment methodologies. *Resilience: The Science of Adaptation to Climate Change*, Elsevier, 3–12.

Sohl, T. L., Dornbierer, J. M., and S. Wilka, 2018: 33 high-resolution scenarios of land use and vegetation change in the Great Plains Landscape Conservation Cooperative region. U.S. Geological Survey data release, https://doi.org/10.5066/F7XW4J03.

Strader, S. M., T. J. Pingel, and W. S. Ashley, 2016: A Monte Carlo model for estimating tornado impacts. *Meteor. Appl.*, **23**, 269–281, https://doi.org/10.1002/met.1552.

——, W. S. Ashley, T. J. Pingel, and A. J. Krmenec, 2017: Projected 21st century changes in tornado exposure, risk, and disaster potential. *Climatic Change*, **141**, 301–313, https://doi.org/10.1007/s10584-017-1905-4.

Szoke, E., M. Weisman, J. Brown, F. Caracena, and T. Schlatter, 1984: A subsynoptic analysis of the Denver tornadoes of 3 June 1981. *Mon. Wea. Rev.*, **112**, 790–808, https://doi.org/10.1175/1520-0493(1984)112<0790:ASAOTD>2.0.CO;2.

Tang, B. H., V. A. Gensini, and C. R. Homeyer, 2019: Trends in United States large hail environments and observations. *npj Climate Atmos. Sci.*, **2**, 45, https://doi.org/10.1038/s41612-019-0103-7.

Taylor, K. E., R. J. Stouffer, and G. A. Meehl, 2012: An overview of CMIP5 and the experiment design. *Bull. Amer. Meteor. Soc.*, **93**, 485–498, https://doi.org/10.1175/BAMS-D-11-00094.1.

Tippett, M. K., J. T. Allen, V. Gensini, and H. E. Brooks, 2015: Climate and hazardous convective wccurr. *Curr. Climate Change Rep.*, **1**, 60–73, https://doi.org/10.1007/s40641-015-0006-6.

Trapp, R. J., and K. A. Hoogewind, 2016: The realization of extreme tornadic storm events under future anthropogenic climate change. *J. Climate*, **29**, 5251–5265, https://doi.org/10.1175/JCLI-D-15-0623.1.

——, N. S. Diffenbaugh, H. E. Brooks, M. E. Baldwin, E. D. Robinson, and J. S. Pal, 2007: Changes in severe thunderstorm environment frequency during the 21st century caused by anthropogenically enhanced global radiative forcing. *Proc. Natl. Acad. Sci. USA*, **104**, 19 719–19 723, https://doi.org/10.1073/pnas.0705494104.

——, E. D. Robinson, M. E. Baldwin, N. S. Diffenbaugh, and B. R. Schwedler, 2011: Regional climate of hazardous convective weather through high-resolution dynamical downscaling. *Climate Dyn.*, **37**, 677–688, https://doi.org/10.1007/s00382-010-0826-y.

——, K. A. Hoogewind, and S. Lasher-Trapp, 2019: Future changes in hail occurrence in the United States determined through convection-permitting dynamical downscaling. *J. Climate*, **32**, 5493–5509, https://doi.org/10.1175/JCLI-D-18-0740.1.

U.S. EPA, 2016: Updates to the demographic and spatial allocation models to produce Integrated Climate and Land Use Scenarios (ICLUS) (version 2). U.S. Environmental Protection Agency External Review Draft EPA/600/R-16/366F, 134 pp.

Verbout, S. M., H. E. Brooks, L. M. Leslie, and D. M. Schultz, 2006: Evolution of the U.S. tornado database: 1954–2003. *Wea. Forecasting*, **21**, 86–93, https://doi.org/10.1175/WAF910.1.

Visser, H., A. Petersen, and W. Ligtvoet, 2014: On the relation between weather-related disaster impacts, vulnerability and climate change. *Climatic Change*, **125**, 461–477, https://doi.org/10.1007/s10584-014-1179-z.

Wilson, J. W., J. A. Moore, G. B. Foote, B. Martner, A. R. Rodi, T. Uttal, and J. M. Wilczak, 1988: Convection Initiation and Downburst Experiment (CINDE). *Bull. Amer. Meteor. Soc.*, **69**, 1328–1347, https://doi.org/10.1175/1520-0477(1988)069<1328:CIADE>2.0.CO;2.

Xie, B., Q. Zhang, and Y. Wang, 2010: Observed characteristics of hail size in four regions in China during 1980–2005. *J. Climate*, **23**, 4973–4982, https://doi.org/10.1175/2010JCLI3600.1.

Yavuz, V., Akbayir, I., Özen, C., and A. Deniz, 2017: Analysis of hail incident for two different provinces in Turkey: A case study using synoptic analysis and numerical weather prediction model (WRF). *Int. J. Eng. Sci.*, **7**, 15 822–15 866.

Zhao, H., and C. Zheng, 2006: Monte Carlo solution of wet removal of aerosols by precipitation. *Atmos. Environ.*, **40**, 1510–1525, https://doi.org/10.1016/j.atmosenv.2005.10.043.